Nonlin. Processes Geophys., 15, 295–304, 2008
www.nonlin-processes-geophys.net/15/295/2008/

Nonlinear Processes in Geophysics

Coronal heating and wind acceleration by nonlinear Alfvén waves – global simulations with gravity, radiation, and conduction

T. K. Suzuki

School of Arts and Sciences, University of Tokyo, Komaba, Meguro, 153-8902 Tokyo, Japan

Received: 10 May 2007 – Revised: 4 January 2008 – Accepted: 15 February 2008 – Published: 26 March 2008

Abstract. We review our recent results of global one-dimensional (1-D) MHD simulations for the acceleration of solar and stellar winds. We impose transverse photospheric motions corresponding to the granulations, which generate outgoing Alfvén waves. We treat the propagation and dissipation of the Alfvén waves and consequent heating from the photosphere by dynamical simulations in a self-consistent manner. Nonlinear dissipation of Alfven waves becomes quite effective owing to the stratification of the atmosphere (the outward decrease of the density). We show that the coronal heating and the solar wind acceleration in the open magnetic field regions are natural consequence of the footpoint fluctuations of the magnetic fields at the surface (photosphere). We find that the properties of the solar wind sensitively depend on the fluctuation amplitudes at the solar surface because of the nonlinearity of the Alfvén waves, and that the wind speed at 1 AU is mainly controlled by the field strength and geometry of flux tubes. Based on these results, we point out that both fast and slow solar winds can be explained by the dissipation of nonlinear Alfvén waves in a unified manner. We also discuss winds from red giant stars driven by Alfvén waves, focusing on different aspects from the solar wind.

1 Introduction

The Alfvén wave, generated by the granulations or other surface activities, is a promising candidate operating in the heating and acceleration of solar winds from coronal holes. It can travel a long distance so that the dissipation plays a role in the heating of the solar wind plasma as well as the lower coronal plasma, in contrast to other processes, such as magnetic reconnection events and compressive waves, the heating of which probably concentrates at lower altitude.

Most of the power of injected Alfvén waves is supposed to be peaked around 5 min ($\sim$0.003 Hz) in the sun, which is, far below the ion cyclotron frequency ($\approx 10^4$ Hz in the corona), in the MHD regime. When considering such low-frequency Alfvén waves in solar and stellar atmospheres, the stratification of the density due to the gravity is quite important because the variation scale of the density, and accordingly Alfvén speed, is comparable to or shorter than the wavelengths; the WKB approximation is no longer applicable. Also, the amplitude of the wave is amplified because of the decrease of the density so that waves easily become nonlinear.

A number of attempts have been carried out to investigate nonlinear Alfvén waves in stratified solar winds in 1-D (Lau and Siregar, 1996; Boynton and Torkelsson, 1996) and 2-D (Ofman and Davila, 1997, 1998; Grappin et al., 2002), and by multi-fluid treatments (Ofman, 2004). These studies nicely explain observations by suitable choices of perturbation amplitude at the inner boundary in the corona. However, the input amplitude at the coronal base is not accurately determined from observations. The photosphere is a more suitable inner boundary for theoretical calculations because the physical properties are precisely obtained from various observations. The density of the coronal base is 8–9 orders of magnitude smaller than that of the photosphere. The dissipation and reflection of Alfvén waves are important in the chromosphere and the transition region, which lie between the photosphere and corona. Furthermore, from the chromosphere to the low corona, radiation cooling plays a role in the energetics. Then, to consistently treat the heating of the gas, the radiative loss needs to be properly taken into account.

Recently, we have extensively studied the heating and acceleration of solar and stellar winds by self-consistent MHD simulations with gravity and cooling (Suzuki and Inutsuka, 2005, 2006; hereafter SI06; Suzuki, 2007). By reviewing

Correspondence to: T. K. Suzuki
(stakeru@ea.c.u-tokyo.ac.jp)

Table 1. Adopted parameters for fast and slow solar wind models.

	$\langle dv_{\perp,0}\rangle$(km s^{-1})	B_0(G)/$f_{\rm tot}$
Fast Wind	0.7	161/75
Slow Wind	1.0	322/450

our recent results, we introduce various aspects of nonlinear Alfvén waves in the Sun and stars to the geophysics community.

2 Set-up

We consider 1-D open flux tubes which are super-radially open, measured by heliocentric distance, r. The simulation regions are from the photosphere (r=1$R_\odot$) with density, ρ=10^{-7} g cm^{-3}, to 65$R_\odot$ (0.3 AU) or $\simeq$20$R_\odot$ ($\simeq$0.1 AU), where $R_\odot$ is the solar radius. Radial field strength, B_r, is given by conservation of magnetic flux as

$$B_r r^2 f(r) = \text{const.}, \tag{1}$$

where $f(r)$ is a super-radial expansion factor. We adopt the same function as in Kopp and Holzer (1976) for $f(r)$ (see SI06 for detail).

We input the transverse fluctuations of the field line by the granulations at the photosphere, which excite Alfvén waves. In this paper we only show results of linearly polarized perturbations with power spectrum proportional to $1/\nu$, where ν is frequency (see SI06 for circularly polarized fluctuations with different spectra). Amplitude, $\langle dv_{\perp,0}\rangle$, at the photosphere is chosen to be compatible with the observed photospheric velocity amplitude $\sim$1 km s^{-1} (Holweger et al., 1978). At the outer boundaries, non-reflecting condition is imposed for all the MHD waves, which enables us to carry out simulations for a long time until quasi-steady state solutions are obtained without unphysical wave reflection.

We dynamically treat the propagation and dissipation of the waves and the heating and acceleration of the plasma by solving ideal MHD equations with the relevant physical processes (paper I):

$$\frac{d\rho}{dt} + \frac{\rho}{r^2 f}\frac{\partial}{\partial r}(r^2 f v_r) = 0, \tag{2}$$

$$\rho\frac{dv_r}{dt} = -\frac{\partial p}{\partial r} - \frac{1}{8\pi r^2 f}\frac{\partial}{\partial r}(r^2 f B_\perp^2) + \frac{\rho v_\perp^2}{2r^2 f}\frac{\partial}{\partial r}(r^2 f) - \rho\frac{GM_\odot}{r^2}, \tag{3}$$

$$\rho\frac{d}{dt}(r\sqrt{f}v_\perp) = \frac{B_r}{4\pi}\frac{\partial}{\partial r}(r\sqrt{f}B_\perp). \tag{4}$$

$$\rho\frac{d}{dt}\left(e + \frac{v^2}{2} + \frac{B^2}{8\pi\rho} - \frac{GM_\odot}{r}\right) + \frac{1}{r^2 f}\frac{\partial}{\partial r}\left[r^2 f\left\{\left(p + \frac{B^2}{8\pi}\right)v_r - \frac{B_r}{4\pi}(\boldsymbol{B}\cdot\boldsymbol{v})\right\}\right] + \frac{1}{r^2 f}\frac{\partial}{\partial r}(r^2 f F_{\rm c}) + q_{\rm R} = 0, \tag{5}$$

$$\frac{\partial B_\perp}{\partial t} = \frac{1}{r\sqrt{f}}\frac{\partial}{\partial r}[r\sqrt{f}(v_\perp B_r - v_r B_\perp)], \tag{6}$$

where ρ, $\boldsymbol{v}$, p, $\boldsymbol{B}$ are density, velocity, pressure, and magnetic field strength, respectively, and subscripts r and $\perp$ denote radial and tangential components; $\frac{d}{dt}$ and $\frac{\partial}{\partial t}$ denote Lagrangian and Eulerian derivatives, respectively; e=$\frac{1}{\gamma-1}\frac{p}{\rho}$ is specific energy and we assume the equation of state for ideal gas with a ratio of specific heat, γ=5/3; G and $M_\odot$ are the gravitational constant and the solar mass; $F_{\rm c}$(=$\kappa_0 T^{5/2}\frac{dT}{dr}$) is thermal conductive flux by Coulomb collisions, where κ_0=10^{-6} in c.g.s unit; q_R is radiative cooling (Landini and Monsignori-Fossi, 1990) (for specific prescription, see SI06).

We adopt the second-order MHD-Godunov-MOCCT scheme (Sano and Inutsuka, 2006) to update the physical quantities. We initially set static atmosphere with a temperature T=10^4 K to see whether the atmosphere is heated up to coronal temperature and accelerated to accomplish the transonic flow. At t=0 we start the inject of the transverse fluctuations from the photosphere and continue the simulations until the quasi-steady states are achieved.

3 Results

3.1 High-speed solar wind

Figure 1 plots the initial condition (dashed lines) and the results after the quasi-steady state condition is achieved at t=2573 min (solid lines), compared with recent observations of fast solar winds. From top to bottom, v_r(km s^{-1}), T(K), mass density, ρ(g cm^{-3}), and rms transverse amplitude, $\langle dv_\perp\rangle$(km s^{-1}) are plotted. As for the density, we compare our result with observed electron density, N_e, in the corona. These variables are averaged for 3 min to incorporate observational exposure time. We set the transverse fluctuation, $\langle dv_{\perp,0}\rangle$=0.7 km s^{-1}, and field strength, $B_{r,0}$=161 G at the photosphere, and the total superradial expansion factor, $f_{\rm tot}$=75 (see Table 1). While our model adopts one-fluid approximation, namely all the species are assumed to be the same temperature and velocity, we think that the temperature represents electrons rather than ions because the temperature is mainly controlled by electron thermal conduction in the corona, and that the velocity represents protons which carry most of the mass.

Figure 1 shows that the initially cool and static atmosphere is effectively heated and accelerated by the dissipation of the Alfvén waves. The sharp transition region which divides the cool chromosphere with $T\sim10^4$ K and the hot corona with $T\sim10^6$ K is formed owing to a thermally unstable region

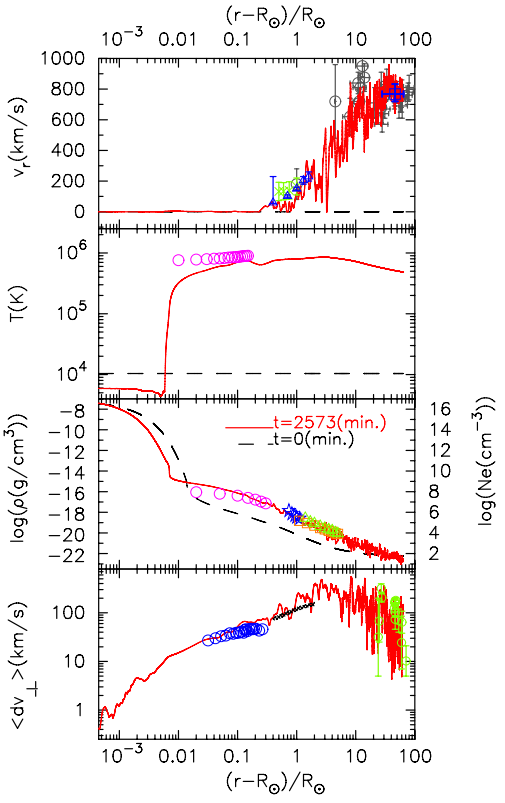

Fig. 1. Results of fast solar wind with observations in polar regions. From top to bottom, outflow speed, v_r(km s^{-1}), temperature, T(K), density in logarithmic scale, log(ρ(g cm^{-3})), and rms transverse amplitude, $\langle dv_\perp \rangle$(km s^{-1}) are plotted. Observational data in the third panel are electron density, log(N_e(cm^{-3})) which is to be referred to the right axis. Dashed lines indicate the initial conditions and solid lines are the results at t=2573 min. In the bottom panel, the initial value ($\langle dv_\perp \rangle$=0) does not appear. *First*: Green vertical error bars are proton outflow speeds in an interplume region by UVCS/SoHO (Teriaca et al., 2003). Dark blue vertical error bars are proton outflow speeds by the Doppler dimming technique using UVCS/SoHO data (Zangrilli et al., 2002). A dark blue open square with errors is velocity by IPS measurements averaged in 0.13–0.3 AU of high-latitude regions (Kojima et al., 2004). Light blue data are taken from Grall et al. (1996); crossed bars are IPS measurements by EISCAT, crossed bars with open circles are by VLBA measurements, and vertical error bars with open circles are data based on observation by SPARTAN 201-01 (Habbal et al., 1994). *Second*: Pink circles are electron temperatures by CDS/SoHO (Fludra et al., 1999). *Third*: Circles and stars are observations by SUMER/SoHO (Wilhelm et al., 1998) and by CDS/SoHO (Teriaca et al., 2003), respectively. Triangles (Teriaca et al., 2003) and squares (Lamy et al., 1997) are observations by LASCO/SoHO. *Fourth*: Blue circles are non-thermal broadening inferred from SUMER/SoHO measurements (Banerjee et al., 1998). Cross hatched region is an empirical constraint of non-thermal broadening based on UVCS/SoHO observation (Esser et al., 1999). Green error bars are transverse velocity fluctuations derived from IPS measurements by EISCAT (Canals et al., 2002).

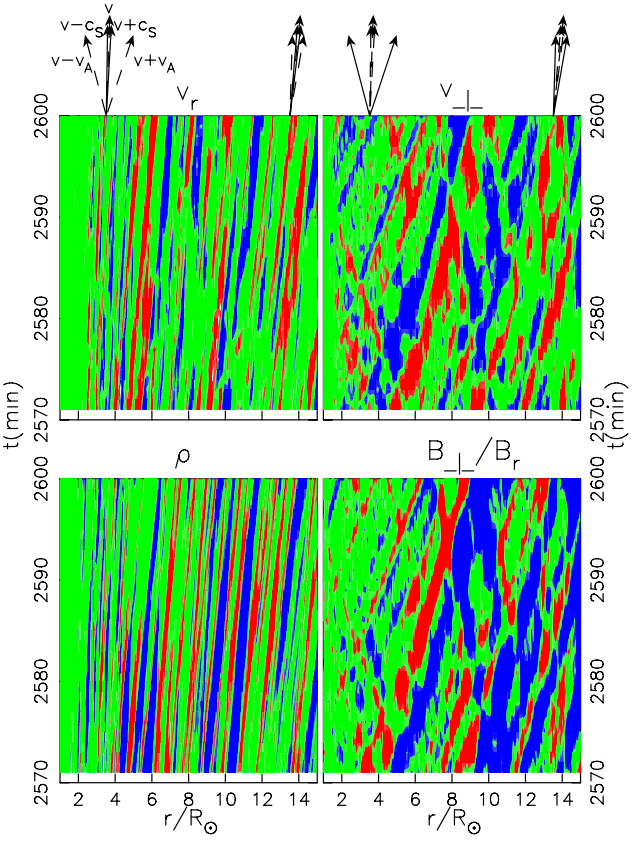

Fig. 2. $r-t$ diagrams for v_r (upper-left), ρ (lower-left), $v_\perp$ (upper-right), and $B_\perp/B_r$ (lower-right.) The horizontal axises cover from $R_\odot$ to $15R_\odot$, and the vertical axises cover from t=2570 min to 2600 min. Dark and light shaded regions indicate positive and negative amplitudes which exceed certain thresholds. The thresholds are dv_r=±96 km/s for v_r, $d\rho/\rho$=±0.25 for ρ, $v_\perp$=±180 km/s for $v_\perp$, and $B_\perp/B_r$=±0.16 for $B_\perp/B_r$, where $d\rho$ and dv_r are differences from the averaged ρ and v_r. Arrows on the top panels indicate characteristics of Alfvén, slow MHD and entropy waves at the respective locations.

around $T\sim10^5$ K in the radiative cooling function (Landini and Monsignori-Fossi, 1990). The hot corona streams out as the transonic solar wind. The simulation naturally explains the observed trend quite well.

The heating and acceleration of the solar wind plasma in inner heliosphere is done by the dissipation of Alfvén waves. Here we inspect waves in more detail. Figure 2 presents contours of amplitude of v_r, ρ, $v_\perp$, and $B_\perp/B_r$ in $R_\odot \le r \le 15R_\odot$ from t=2570 min to 2600 min. Red (blue) shaded regions denote positive (negative) amplitude. Above the panels, we indicate the directions of the local 5 characteristics, two Alfvén, two slow, and one entropy waves at the respective positions. Note that the fast MHD and Alfvén modes degenerate in our case (wave vector and underlying magnetic field are in the same direction), so we simply call the innermost and outermost waves Alfvén modes. In our simple 1-D

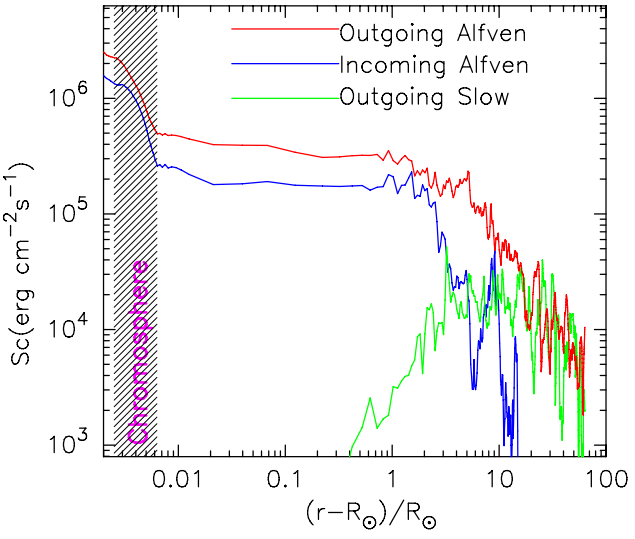

Fig. 3. S_c of outgoing Alfvén mode (red), incoming Alfvén mode (blue), and outgoing MHD slow mode (green) at t=2573 min. Hatched region indicates the chromosphere and low transition region with $T<4\times10^4$ K.

geometry, v_r and ρ trace the slow modes which have longitudinal wave components, while $v_\perp$ and $B_\perp$ trace the Alfvén modes which are transverse.

One can clearly see the Alfvén waves in $v_\perp$ and $B_\perp/B_r$ diagrams, which have the same slopes with the Alfvén characteristics shown above. One can also find the incoming modes propagating from lower-right to upper-left as well as the outgoing modes generated from the surface. These incoming waves are generated by the reflection at the 'density mirrors' of the slow modes. At intersection points of the outgoing and incoming characteristics the non-linear wave-wave interactions take place, which play a role in the wave dissipation.

The slow modes are seen in v_r and ρ diagrams. Although it might be difficult to distinguish, most of the patterns are due to the outgoing slow modes[1] which are generated from the perturbations of the Alfvén wave pressure, $B_\perp^2/8\pi$ (Kudoh and Shibata, 1999). These slow waves steepen eventually and lead to the shock dissipation.

Figure 3 presents the dissipation of the waves more quantitatively. It plots the following quantities,

$$S_c = \rho\delta v^2 \frac{(v_r + v_{\rm ph})^2}{v_{\rm ph}} \frac{r^2 f(r)}{r_c^2 f(r_c)}, \quad (7)$$

of outgoing Alfvén, incoming Alfvén, and outgoing slow MHD (sound) waves, where δv and $v_{\rm ph}$ are amplitude and phase speed of each wave mode. S_c is an adiabatic constant in unit of energy flux derived from wave action (Jacques, 1977). For the incoming Alfvén wave, we plot the opposite sign of S_c so that it becomes positive in the sub-Alfvénic region. The outgoing and incoming Alfvén waves are decomposed by correlation between $v_\perp$ and $B_\perp$. Extraction of the slow wave is also from fluctuating components of v_r and ρ.

Figure 3 clearly illustrates that slow MHD waves as well as incoming Alfvén waves are nonlinearly generated, which play a role in the heating and acceleration of the solar wind plasma. Then, the outgoing Alfvén waves dissipate quite effectively; S_c becomes only $\sim10^{-3}$ of the initial value at the outer boundary. Figure 3 also shows that a sizable amount is reflected back downward below the coronal base ($r-R_\odot<0.01R_\odot$), which is clearly illustrated as the incoming Alfvén wave following the outgoing component with slightly smaller level. This is because the wave shape is considerably deformed owing to the steep density gradient; a typical variation scale ($<10^5$ km) of the Alfvén speed becomes comparable to or even shorter than the wavelength (=10^4-10^6 km). Although the energy flux, $\simeq5\times10^5$ erg cm^{-2} s^{-1}, of the outgoing Alfvén waves (S_c in the static region is equivalent with the energy flux) which penetrates into the corona is only $\simeq$15% of the input value, it satisfies the requirement for the energy budget in the coronal holes (Withbroe and Noyes, 1977).

The processes discussed here are the combination of the direct mode conversion to the compressive waves and the parametric decay instability due to three-wave (outgoing Alfvén, incoming Alfvén, and outgoing slow waves) interactions (Goldstein, 1978; Terasawa et al., 1986) of the Alfvén waves. Although they are not generally efficient in the homogeneous background since they are the nonlinear mechanisms, the density gradient of the background plasma totally changes the situation. Owing to the gravity, the density rapidly decreases in the corona as r increases, which results in the amplification of the wave amplitude so that the waves easily become nonlinear. Furthermore, the Alfvén speed varies a lot due to the change of the density even within one wavelength of Alfvén waves with periods of minutes or longer. This leads to both variation of the wave pressure in one wavelength and partial reflection through the deformation of the wave shape (Moore et al., 1991). The dissipation is greatly enhanced by the density stratification, in comparison with the case of the homogeneous background. Thus, the low-frequency Alfvén waves are effectively dissipated, which results in the heating and acceleration of the coronal plasma.

Before closing this section, it should be noted that the above discussion is based on the 1-D simulation. In realistic 3-D treatments, various other dissipation channels become effective, which will be discussed in Sect. 4.

[1]The phase correlation of the longitudinal slow waves is opposite to that of the transverse Alfvén waves. The outgoing slow modes have the positive correlation between amplitudes of v_r and ρ, ($\delta v_r\delta\rho>0$), while the incoming modes have the negative correlation ($\delta v_r\delta\rho<0$).

3.2 Dependence on dv

We study dependences on the amplitudes of the input fluctuations at the photosphere. We compare the results of larger $\langle dv_{\perp,0}\rangle$=1.4 km s^{-1} and smaller $\langle dv_{\perp,0}\rangle$=0.4 km s^{-1} and 0.3 km s^{-1} cases with the fiducial case ($\langle dv_{\perp,0}\rangle$=0.7 km s^{-1}) in Fig. 4. Note in the case of $\langle dv_{\perp,0}\rangle$=0.3 km s^{-1} quasi steady-state behavior is not achieved, and the density and temperature decrease with time as explained later.

The maximum temperature of $\langle dv_{\perp,0}\rangle$=0.4 km s^{-1} case is $\simeq 5\times10^5$ K, which is cooler than the usual corona. The density is much lower than the fiducial case by 1–2 orders of magnitude because the sufficient mass cannot supply into the corona by the chromospheric evaporation owing to the low temperature; the evaporation is drastically suppressed as T decreases since the conductive flux ($F_c \propto T^{5/2}\frac{dT}{dr}$) sensitively depends on T. As a result, the mass flux (ρv_r) becomes more than an order of magnitude lower than that of the present solar wind. These tendencies are more extreme in the $\langle dv_{\perp,0}\rangle$=0.3 km s^{-1} case; the coronal temperature and density become further low in the case of $\langle dv_{\perp,0}\rangle$=0.3 km s^{-1}; $T\simeq 2\times10^5$ K and the density in the corona and solar wind is smaller by 3 orders of magnitude than the fiducial case.

This behavior can be understood by the wave dissipation. The Alfvén speed ($=B/\sqrt{4\pi\rho}$) is larger in a smaller $\langle dv_{\perp,0}\rangle$ case due to the lower density and the nonlinearity, $\langle \delta v_{A,+}\rangle / v_A$, becomes weaker. As a result, the final energy flux of the solar wind at 0.1 AU, mostly consisting of the kinetic energy ($\rho v_r \frac{v_r^2}{2}$), becomes further smaller compared to the difference of input energy flux.

Once the coronal density starts to decrease, a positive feedback operates. Namely, the decrease of the density leads to weaker non-linearity of the Alfvén waves, which reduces the plasma heating by the wave dissipation. This decreases the coronal temperature, and further reduces the coronal density by the suppression of the chromospheric evaporation. This takes place in the case of $\langle dv_{\perp,0}\rangle$=0.3 km s^{-1} so that the coronal density and temperature continue to decrease at later time, instead of maintaining steady corona and solar wind.

Our results show that $\langle dv_{\perp,0}\rangle \gtrsim 0.4$ km s^{-1} is the criterion of the photospheric fluctuations for the formation of the stable hot plasma. To get the maximum coronal temperature $\gtrsim 10^6$ K, $\langle dv_{\perp,0}\rangle \gtrsim 0.7$ km s^{-1} is required. Otherwise if $\langle dv_{\perp,0}\rangle \lesssim 0.3$ km s^{-1}, the low-frequency Alfvén waves cannot maintain the hot corona, and the solar wind mass flux becomes drastically small.

Larger $\langle dv_{\perp,0}\rangle$ gives larger coronal density. The initial increase of the temperature starts from a deeper location around $r\simeq 0.005 R_\odot$ than the other cases. Thanks to this, a decrease of the density is slower (larger pressure scale height) so that the density around r=1.01$R_\odot$ is two orders of magnitude larger than that of the case with $\langle dv_{\perp,0}\rangle$=0.7 km s^{-1}. However, the temperature decreases slightly instead of a monotonical increase; it cannot go over the peak of the radiative cooling function at $T\simeq 10^5$ K (Landini and Monsignori-Fossi, 1990) because the radiative loss is efficient owing to the large density. The second increase of the temperature begins from $r\simeq 1.03 R_\odot$ and above there the corona is formed. The coronal density and temperature are larger than those in the case with $\langle dv_{\perp,0}\rangle$=0.7 km s^{-1}. In particular the density in the outer region is 10 times larger, and the mass flux of the solar wind is larger by the same extent.

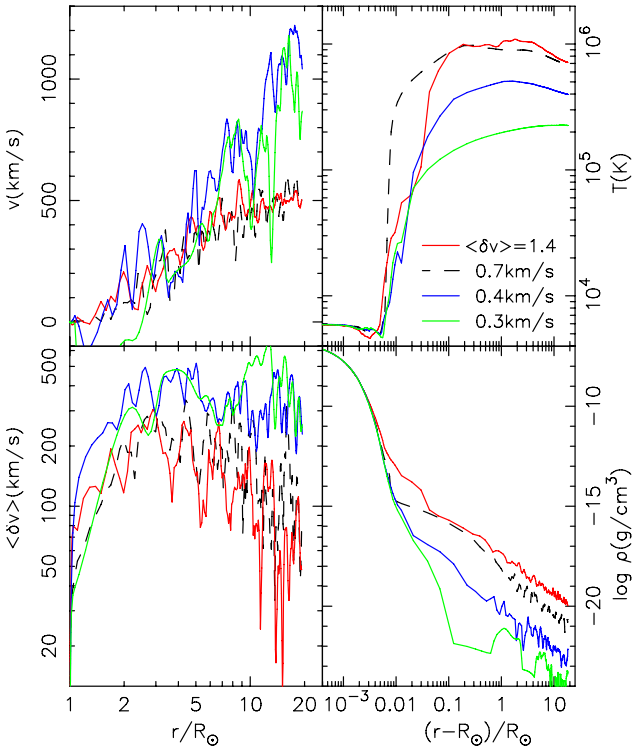

Fig. 4. Structures of corona and solar wind for different $\langle dv_\perp\rangle$=0.3 (green), 0.4 (blue), 0.7 (black dashed), and 1.4 km s^{-1} (red). We plot solar wind speed, v_r(km s^{-1}) (top left), temperature, T(K) (top right), density in logarithmic scale, log(ρ(g cm^{-3})) (bottom right), and rms transverse velocity, $\langle dv_\perp\rangle$(km s^{-1}) (bottom left). Each variable is averaged with respect to time during 28 min (the longest wave period considered).

3.3 Solar wind speed

It is widely believed that field strength and geometry of open flux tubes are important parameters that control the solar wind speed. Wang and Sheeley (1990, 1991) showed that the solar wind speed at ~1 AU is anti-correlated with f_{tot} from their long-term observations as well as by a simple theoretical model. Ofman and Davila (1998) showed this tendency by time-dependent simulations as well. Fisk et al. (1999) claimed that the wind speed should be positively correlated with $B_{r,0}$ by a simple energetics consideration.

Kojima et al. (2005) have found that the solar wind velocity is better correlated with the combination of these two

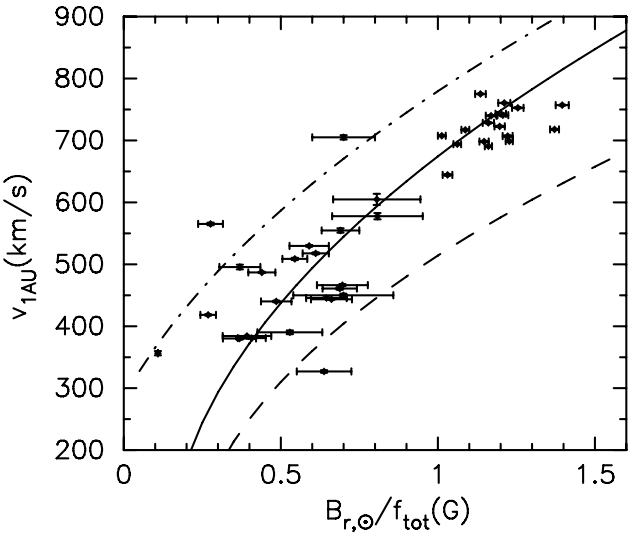

Fig. 5. Relations between $v_{1\,\mathrm{AU}}$ and $B_{r,\odot}/f_{\mathrm{tot}}$. Lines are theoretical prediction from Eq. (8). Solid line indicates the fiducial case ($\langle\delta B_\perp \delta v_\perp\rangle$=$8.3\times10^5$ G cm s^{-1} and T_{C}=10^6 K). Dot-dashed line adopt higher coronal temperature (T_{C}=1.5×10^6 K) with the fiducial $\langle\delta B_\perp \delta v_\perp\rangle$. Dashed line adopt smaller $\langle\delta B_\perp \delta v_\perp\rangle$ (=5.3×10^5 G cm s^{-1}) with the fiducial temperature. Observed data are from Kojima et al. (2005). Coronal magnetic fields are extrapolated from $B_{r,\odot}$ by the potential field-source surface method (Hakamada and Kojima, 1999). f_{tot} is derived from comparison between the areas of open coronal holes at the photosphere and at the source surface (r=$2.5R_\odot$). $v_{1\,\mathrm{AU}}$ is obtained by interplanetary scintillation measurements. $v_{1\,\mathrm{AU}}$, $B_{r,\odot}$, and f_{tot} are averaged over the area of each coronal hole and the data points correspond to individual coronal holes.

parameters, $B_{r,0}/f_{\mathrm{tot}}$, than $1/f_{\mathrm{tot}}$ or $B_{r,0}$ from the comparison of the outflow speed obtained by their interplanetary scintillation measurements with observed photospheric field strength (Fig. 5). Suzuki (2004), SI06 and Suzuki (2006) also pointed out that $B_{r,0}/f_{\mathrm{tot}}$ should be the best control parameter provided that the Alfvén waves play a dominate role in the coronal heating and the solar wind acceleration. This is because the nonlinearity of the Alfvén waves, $\langle\delta v_{\mathrm{A},+}\rangle/v_{\mathrm{A}}$ is controlled by $v_{\mathrm{A}}\propto B_r\propto B_{r,0}/f_{\mathrm{tot}}$ in the outer region where the flux tube is already super-radially open. Wave energy does not effectively dissipate in the larger $B_{r,0}/f_{\mathrm{tot}}$ case in the subsonic region because of relatively small nonlinearity and more energy remains in the supersonic region. In general, energy and momentum inputs in the supersonic region gives higher wind speed, while those in the subsonic region raises the mass flux (ρv_r) of the wind by an increase of the density (Lamers and Cassinelli, 1999). This indicates that the solar wind speed is positively correlated with $B_{r,0}/f_{\mathrm{tot}}$.

Suzuki (2006) further derived a relation between the solar wind speed, $v_{1\,\mathrm{AU}}$, at 1 AU and surface properties from a simple energetics argument:

$$v_{1\,\mathrm{AU}} = \left[2\times\left(-\frac{R_\odot^2}{4\pi(\rho v r^2)_{1\,\mathrm{AU}}}\frac{B_{r,\odot}}{f_{\mathrm{tot}}}\langle\delta B_\perp\delta v_\perp\rangle_\odot + \frac{\gamma}{\gamma-1}RT_{\mathrm{C}} - \frac{GM_\odot}{R_\odot}\right)\right]^{1/2} \quad (8)$$
$$= 300(\mathrm{km/s})\left[5.9\left(\frac{-\langle\delta B_\perp\delta v_\perp\rangle_\odot}{8.3\times10^5(\mathrm{cm\ s^{-1}G})}\right)\left(\frac{B_{r,\odot}(\mathrm{G})}{f_{\mathrm{tot}}}\right) + 3.4\left(\frac{\gamma}{1.1}\right)\left(\frac{0.1}{\gamma-1}\right)\left(\frac{T_{\mathrm{C}}}{10^6(\mathrm{K})}\right) - 4.2\right]^{1/2},$$

where we have the three free parameters, surface amplitude, $\langle\delta B_\perp\delta v_\perp\rangle_\odot$, *effective* coronal temperature, T_{C}, and ratio of specific heats, γ. In the equation, these parameters are evaluated by the standard values, which should be used for actual prediction of wind speed. The first term is the contribution from Alfvén waves, the second term represents net heating minus cooling due to radiation loss and thermal conduction, and the third term is the gravitational loss. The first term, due to Alfvén waves, exhibits the dependence on $B_{r,0}/f_{\mathrm{tot}}$, which reflects the Alfvén waves in expanding flux tubes. Figure 5 shows the prediction of Eq. (8), in comparison with the observation using interplanetary scintillation measurements by Kojima et al. (2005). The observed data are nicely explained by the relation based on the simple energetics.

3.4 Unification of high-/low-speed solar winds

Based on our studies we can infer the suitable $\langle dv_{\perp,0}\rangle$ and $B_{r,0}/f_{\mathrm{tot}}$ for the slow solar wind by comparing with those of the fast wind: The slow wind requires larger $\langle dv_{\perp,0}\rangle$ and smaller $B_{r,0}/f_{\mathrm{tot}}$ than the fast wind. The adopted parameters are summarized in Table 1.

Figure 6 presents the results of fast (dashed lines) and slow (solid lines) solar winds overlayed with recent observations. The temperature and density of the slow wind case becomes larger on account of the larger $\langle dv_{\perp,0}\rangle$, which explains the observations. On the other hand, smaller B_0/f_{tot} gives slower terminal speed. As a result, the observed anti-correlation of the wind speed and the coronal temperature (Schwadron and McComas, 2003) is well-explained by our simulations. In the slow wind case, the acceleration of the outflow is more gradual, and it is not negligible in $r\gtrsim20\,R_\odot$ (e.g. Nakagawa et al., 2006).

The Alfvén wave dissipates more slowly in the fast wind conditions because of larger $B_r(\propto B_{r,0}/f_{\mathrm{tot}})$. As a result, $\langle dv_\perp\rangle$ is larger in the fast wind model. Various in situ observations in the solar wind plasma near the earth also show that the fast wind contains more Alfvénic wave components (see Tsurutani and Ho, 1999, for review), which can be explained via the nonlinear dissipation of Alfvén waves based on our simulations.

Although $\langle dv_{\perp,0}\rangle$ and $B_{r,0}/f_{\mathrm{tot}}$ of the fast and slow winds are simply chosen to explain the observations, we would like

to discuss the difference of these parameters. Slow winds are mainly from low-latitude regions, which are mostly covered by closed regions. Then, open field regions in low-latitude regions generally expand more, namely $f_{\rm tot}$ is larger. This is an interpretation why $B_0/f_{\rm tot}$ is smaller in slow winds. Some solar winds are known from the vicinity of active regions (Kojima et al., 1999). Due to the influence from active regions, the amplitudes of the footpoint motions of these solar winds is expected to be larger than solar winds originating from coronal holes. We think that this leads to larger $\langle dv_{\perp,0}\rangle$ in slow winds.

3.5 Application to red giant winds

So far we have focused on the acceleration of solar wind. However, the same process is expected to operate in other types of stars that have surface convective layer, such as red giant stars, proto-stars, and intermediate and low mass main sequence stars. Red giant winds are studied in 1-D steady-state calculations (Hartmann and MacGregor , 1980) and 2-D dynamical simulations (Airapetian et al., 2000), although these studies do not set photosphere as the inner boundaries but arbitrary higher altitudes. We simulation red giant winds from the photosphere by extending the solar wind simulation (Suzuki, 2007).

We consider stellar winds from $1M_\odot$ stars in various evolutionary stages from main sequence to red giant branch. The properties of surface fluctuations (e.g. amplitude and spectrum) can be estimated from conditions of surface convection which depend on surface gravity and temperature (e.g. Renzini et al., 1977; Stein et al., 2004). Then, we carry out the simulations of the red giant winds in a similar manner to the solar wind simulations.

Figure 7 presents the evolution of stellar winds of a $1M_\odot$ star from main sequence to red giant stages. The middle panel shows that the average temperature drops suddenly from $T\simeq 7\times10^5$ K in the sub-giant star (blue) to $T\leq 10^5$ K in the red giant stars, which is consistent with the observed "dividing line" (Linsky and Haisch, 1979). The main reason of the disappearance of the steady hot coronae is that the sound speed ($\approx$150 km s^{-1}) of $\approx 10^6$ K plasma exceeds the escape speed, $v_{\rm esc}(r)=\sqrt{2GM_\star/r}$, at $r\gtrsim$ a few $R_\star$ in the red giant stars; the hot corona cannot be confined by the gravity any more in the atmospheres of the red giant stars. Therefore, the material flows out before heated up to coronal temperature. In addition, the thermal instability of the radiative cooling function (Landini and Monsignori-Fossi, 1990) plays a role in the sudden decrease of temperature (Suzuki, 2007).

The top panel of Fig. 7 shows that nearly-static regions are formed above the photospheres in the red giant stars, and the acceleration of the winds essentially starts from several stellar radii. Accordingly, their wind speeds in the outer regions are considerably slower than the escape velocities at the surfaces, which is consistent with the observed trend (e.g. Dupree, 1986).

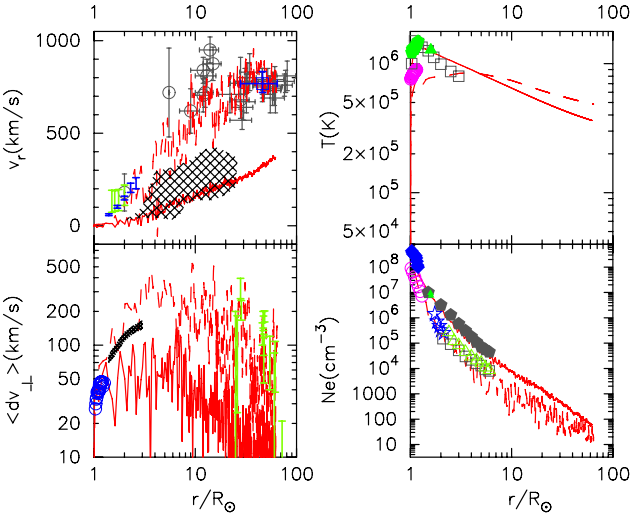

Fig. 6. Simulation results of the fast (dashed) and slow (solid) solar wind models in comparison with observations. Outflow velocity, v_r(km s^{-1}) (top left), temperature, T(K) (top right), electron density, N_e(cm^{-3}) (bottom right), and rms transverse velocity, $\langle dv_\perp\rangle$(km s^{-1}) (bottom left) are plotted. The observations in polar regions to be compared with the fast wind model are shown by open symbols, and the data in mid- to low-latitude region for the slow wind modes are by filled symbols. Since the data for the fast wind are the same as in Fig. 1, we summarize the data for the slow wind below. *Observational data; top-left*: Shaded region is observational data in the streamer belt (Sheeley et al., 1997). *Top-right*: Filled diamonds and triangles are electron temperature obtained from the line ratio of Fe XIII/X in the mid-latitude streamer by CDS/SOHO and UVCS/SOHO respectively (Parenti et al., 2000). *Bottom-right*: Filled diamonds and triangles are data respectively from CDS and UVCS on SOHO observation of the mid-latitude streamer (Parenti et al., 2000), and filled pentagons derived from observation of the total brightness in the equator region by LASCO/SOHO (Hayes et al., 2001).

4 Discussion

In this paper we treat wave propagation and dissipation within 1-D MHD approximation, of which validity needs to be cautiously examined. Solar wind plasma around 1 AU shows complicated structures. Various types of discontinuities are observed, which are regarded as a result of phase steepening or turbulent-like cascade of nonlinear Alfvén waves (Tsurutani et al., 2002, 2005). Multi-dimensionality, which enhances turbulent cascade (Goldreich and Sridhar, 1995; Oughton et al., 2001), and/or effects beyond MHD, e.g. finite Larmor radius effect, are supposed to be important in these events. Probably, these complicated structures also play a role in the dissipation of Alfvén waves in the inner heliopshere. It is important to quantitatively estimate how these processes operate in the actual solar and stellar winds besides the 3-wave process we are discussing in this paper.

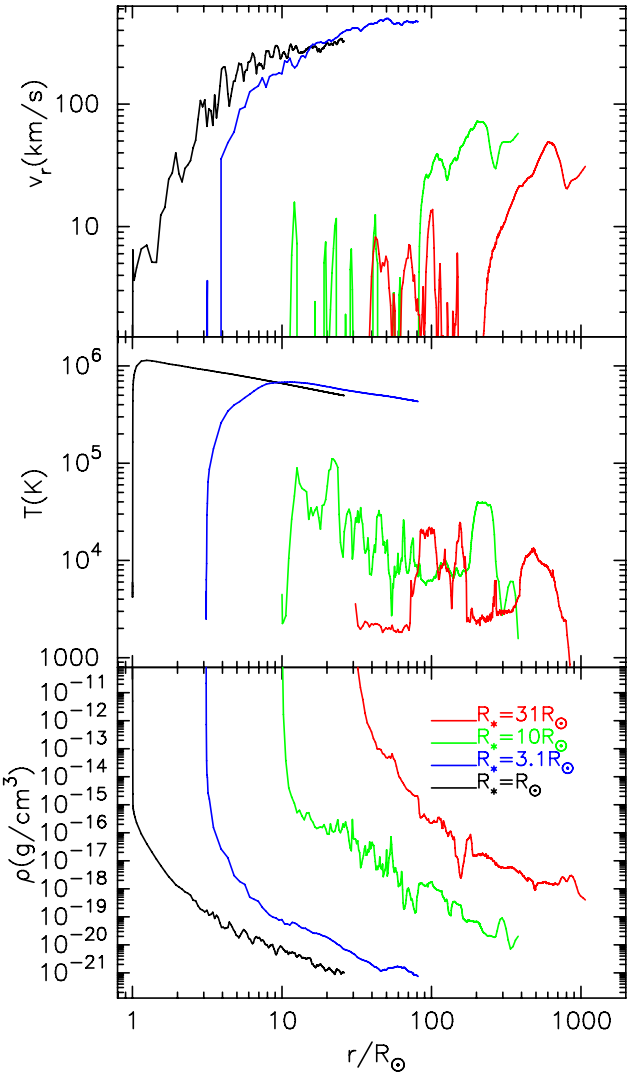

Fig. 7. Time-averaged stellar wind structure of the $1M_\odot$ stars. From the top to the bottom, radial outflow velocity, v_r (km s^{-1}), temperature, T (K), and density, ρ (g cm^{-3}), are plotted. The black, blue, green, and red lines are the results of stellar radii, R=$R_\odot$ (the present Sun), $3.1R_\odot$ (sub-giant), $10R_\odot$ (red giant), and $31R_\odot$ (red giant), respectively.

If Alfvén waves cascade to higher frequency (Chandran, 2005), kinetic effects (e.g. Nariyuki and Hada, 2006) becomes important. The high-frequency ($\sim 10^4$ Hz in the solar corona and $\sim$1–10 Hz at $\approx$0.3 AU in the solar wind) ion cyclotron waves were recently highlighted for the additional heating of minor heavy ions (e.g. O, Mg) (Axford and McKenzie, 1997; Kohl et al., 1998). The resonant frequency, which is in proportion to mass-to-charge ratio, is smaller for heavy ions. As a result, these ions are heated up before protons by resonant coupling with ion cyclotron waves. This process results in the perpendicular heating with respect to underlining field, which is actually observed in heavy ions. However, it is difficult to heat up protons which compose the main part of plasma because the energy of ion cyclotron waves that are resonantly coupled with protons are already absorbed by the heavy ions (Cranmer, 2000). Therefore, we believe that low frequency ($\lesssim$1 Hz) Alfvén waves, which are focusing on in this paper, is more dominant in the total heating.

5 Conclusions

We have performed 1-D MHD numerical simulations of solar and stellar winds from the photosphere. The low-frequency Alfvén waves are generated by the footpoint fluctuations of the magnetic field lines. We have treated the wave propagation and dissipation, and the heating and acceleration of the plasma in a self-consistent manner. Our simulation is the first simulation which treats the wind from the real surface (photosphere) to the (inner) heliosphere with the relevant physical processes.

We have shown that the dissipation of the low-frequency Alfvén waves through the generation of the compressive waves (decay instability) and shocks (nonlinear steepening) is one of the solutions for the heating and acceleration of the plasma in the coronal holes. However, we need to carefully examine the validity of the 1-D MHD approximation we have adopted.

The density, and accordingly the mass flux, of solar winds show a quite sensitive dependence on $\langle dv_{\perp,0}\rangle$ because of an unstable aspect of the heating by the nonlinear Alfvén waves. For example, the mass flux of solar wind becomes $\sim$100 times smaller if $\langle dv_{\perp,0}\rangle$ becomes $\simeq$1/2. We also find that the solar wind speed has a positive correlation with $B_{r,0}/f_{\rm tot}$, which is consistent with recent observations by Kojima et al. (2005).

Based on these findings, we show that both fast and slow solar winds can be explained by the single process, the dissipation of the nonlinear low-frequency Alfvén waves, with different sets of $\langle dv_{\perp,0}\rangle$ and $B_{r,0}/f_{\rm tot}$. Our simulations naturally explain the observed (i) anti-correlation of the solar wind speed and the coronal temperature and (ii) larger amplitude of Alfvénic fluctuations in the fast wind.

We have also extended the solar wind simulations to red giant winds. With stellar evolution, the steady hot corona with temperature, $T\approx 10^6$ K, suddenly disappears because the surface gravity becomes small; hot plasma cannot be confined by the gravity. Nearly static regions are formed above the photospheres of the red giant stars, and the stellar winds are effectively accelerated from several stellar radii. Then, the wind velocity is much smaller than the surface escape speed, because it is regulated by the slower escape speed at that location.

Acknowledgements. The author thanks the organizers of NLW6 for the nice conference. The author also thanks the referees for valuable comments. This work is supported in part by a Grant-in-Aid for Scientific Research (18840009) from the Ministry of Education, Culture, Sports, Science, and Technology of Japan.

Edited by: T. Hada
Reviewed by: two anonymous referees

References

Airapetian, V. S., Ofman, L., Robinson, R. D., Carpenter, K., and Davila, J.: Winds from Luminous Late-Type Stars. I. The Effects of Nonlinear Alfvén Waves, Astrophys. J., 528, 965–971, 2000.

Axford, W. I. and McKenzie, J. F.: The Solar Wind, in: Cosmic Winds and the Heliosphere, edited by: Jokipii, J. R., Sonnet, C. P., and Giampapa, M. S., University of Arizona Press, 31–66, 1997.

Banerjee, D., Teriaca, L., Doyle, J. G., and Wilhelm, K.: Broadening of SI VIII lines observed in the solar polar coronal holes, Astron. Astrophys., 339, 208–214, 1998.

Boynton, G. C. and Torkelsson, U.: Dissipation of nonlinear Alfvén waves, Astron. Astrophys., 308, 299–308, 1996.

Canals, A., Breen, A. R., Ofman, L., Moran, P. J., and Fallows, R. A.: Estimating random transverse velocities in the fast solar wind from EISCAT interplanetary scintillation measurements, Ann. Geophys., 20, 1265–1277, 2002, http://www.ann-geophys.net/20/1265/2002/.

Chandran, B. D. G.: Weak Compressible Magnetohydrodynamic Turbulence in the Solar Corona Phys. Rev. Lett., 95, 265004, 2005.

Cranmer, S. R.: Ion cyclotron wave dissipation in the solar corona: Astrophys, J., 532, 1197–1208, 2000.

Dupree, A. K.: Mass Loss from Cool Stars, Ann. Rev. Astron. Astrophys., 24, 377–420, 1986.

Esser, R., Fineschi, S., Dobrzycka, D., Habbal, S. R., Edgar, R. J., Raymond, J. C., and Kohl, J. L.: Plasma properties in coronal holes derived from measurements of minor ion spectral lines and polarized white light intensity, Astrophys. J. Lett., 510, L63–L67, 1999.

Fisk, L. A., Schwadron, N. A., and Zurbuchen, T. H.: Acceleration of the fast solar wind by the emergence of new magnetic flux, J. Geophys. Res., 104(A4), 19 765–19 772, 1999.

Fludra, A., Del Zanna, G., and Bromage, B. J. I.: EUV observations above polar coronal holes, Space Sci. Rev., 87, 185–188, 1999.

Goldreich, P. and Sridhar, S.: Toward a theory of interstellar turbulence. 2: Strong Alfvénic turbulence, Astrophys. J., 438, 763–775, 1995.

Goldstein, M. L.:, An instability of finite amplitude circularly polarized Alfvén waves, Astrophys. J., 219, 700–704, 1978.

Grall, R. R., Coles, W. A., Klinglesmith, M. T., Breen, A. R., Williams, P. J. S., Markkanen, J., and Esser, R.: Rapid acceleration of the polar solar wind, Nature, 379, 429–432, 1996.

Grappin, R., Léorat, J., and Habbal, S. R.: Large-amplitude Alfvén waves in open and closed coronal structures: A numerical study, J. Geophys. Res., 107(A11), 1380, doi:10.1029/2001JA005062, 2002.

Habbal, S. R., Esser, R., Guhathakura, M., and Fisher, R. R.: Flow properties of the solar wind derived from a two-fluid model with constraints from white light and in situ interplanetary observations, Gephys. Res. Lett., 22, 1465–1468, 1994.

Hakamada, K. and Kojima, M.: Solar Wind Speed and Expansion Rate of the Coronal Magnetic Field during Carrington Rotation 1909, Sol. Phys., 187, 115–122, 1999.

Hartmann, L. and MacGregor, K. B.: Momentum and energy deposition in late-type stellar atmospheres and winds, Astrophys. J., 242, 260–282, 1980.

Hayes, A. P., Vourlidas, A., and Howard, R. A.: Deriving the Electron Density of the Solar Corona from the Inversion of Total Brightness Measurements, Astrophys. J., 548, 1081–1086, 2001.

Holweger, H., Gehlsen, M., and Ruland, F.: Spatially-averaged properties of the photospheric velocity field, Astron. Astrophys., 70, 537–542, 1978.

Jacques, S. A.: Momentum and energy transport by waves in the solar atmosphere and solar wind, Astrophys. J., 215, 942–951, 1977.

Kohl, J. L., Noci, G., Antonucci, E., et al.: UVCS/SOHO empirical determinations of anisotropic velocity distributions in the solar corona, Astrophys. J. Lett., 501, L127–L131, 1998.

Kojima, M., Fujiki, K., Ohmi, T., Tokumaru, M., Yokobe, A., and Hakamada, K.: Low-speed solar wind from the vicinity of solar active regions, J. Geophys. Res., 104, 16 993–17 004, 1999.

Kojima, M., Breen, A. R., Fujiki, K., Hayashi, K., Ohmi, T., and Tokumaru, M.: Fast solar wind after the rapid acceleration, J. Geophys. Res., 109, A04103, doi:10.1029/2003JA010247, 2004.

Kojima, M., Fujiki, K., Hirano, M., Tokumaru, M., Ohmi, T., and Hakamada, K.: Solar Wind properties from IPS observations, in: The Sun and the heliosphere as an Integrated System, edited by: Poletto, G. and Suess, S. T., Kluwer Academic Publishers, 147–181, 2005.

Kopp, R. A. and Holzer, T. E.: Dynamics of coronal hole regions. I – Steady polytropic flows with multiple critical points, Sol. Phys., 49, 43–56, 1976.

Kudoh, T. and Shibata, K.: Alfvén wave model of spicules and coronal heating, Astrophys. J., 514, 493–505, 1999.

Lamers, H. J. G. L. M. and Cassinelli, J. P.: Introduction to Stellar Wind, Cambridge, 1999.

Lamy, P., Quemerais, E., Liebaria, A., Bout, M., Howard, R., Schwenn, R., and Simnett, G.: Characterization of Polar Plumes from LASCO-C2 Images in Early 1996, in: Fifth SOHO Worshop, The Corona and Solar Wind near Minimum Activity, edited by: Wilson, A., ESA-SP 404; Noordwijk:ESA, 491, 1997.

Landini, M. and Monsignori-Fossi, B. C.: The X-UV spectrum of thin plasmas, Astron. Astrophys. Supp., 82, 229–260, 1990.

Lau, Y.-T. and Siregar, E.: Nonlinear Alfvén waves, Astrophys. J., 465, 451–461, 1996.

Linsky, J. L. and Haisch, B. M.: Outer atmospheres of cool stars. I – The sharp division into solar-type and non-solar-type stars, Astrophys. J. Lett., 229, L27–L32, 1979.

Moore, R. L., Suess, S. T., Musielak, Z. E., and An, A.-H.: Alfvén wave trapping, network microflaring, and heating in solar coronal holes, Astrophys. J., 378, 347–359, 1991.

Nakagawa, T., Gopalswamy, N., and Yashiro, S.: Solar wind speed within $20R_S$ of the sun estimated from limb CMEs, J. Geophys. Res., 111, A01108, doi:10.1029/2005JA011249, 2006.

Nariyuki, Y. and Hada, T.: Kinetically modified parametric instabilities of circularly polarized Alfvén waves: Ion kinetic effects, Phys. Plasma, 13, 12450-1–14501-4, 2006.

Ofman, L.: Three-fluid model of the heating and acceleration of the fast solar wind, J. Geophys. Res., 109, A07102, doi:10.1029/2003JA010221, 2004.

Ofman, L. and Davila, J. M.: Solar Wind Acceleration by Solitary Waves in Coronal Holes, Astrophys. J., 476, 357–365, 1997.

Ofman, L. and Davila, J. M.: Solar wind acceleration by large-amplitude nonlinear waves: Parametric study, J. Geophys. Res., 103, 23 677–23 690, 1998.

Oughton, S., Matthaeus, W. H., Dmitruk, P., Milano, L. J., Zank, G. P., and Mullan, D. J.: A reduced magnetohydrodynamic model of coronal heating in open magnetic regions driven by reflected low-frequency Alfvén waves, Astrophys. J., 551, 565–575, 2001.

Parenti, S., Bromage, B. J. I., Poletto, G., Noci, G., Raymond, J. C., and Bromage, G. E.: Characteristics of solar coronal streamers. Element abundance, temperature and density from coordinated CDS and UVCS SOHO observations, Astron. Astrophys., 363, 800–814, 2000.

Renzini, A., Cacciari, C., Ulmschneider, P., and Schmitz, F.: Theoretical chromospheres of late type stars. I – Acoustic energy generation, Astron. Astrophys., 61, 39–45, 1977.

Schwadron, N. A. and McComas, D. J.: Solar Wind Scaling Law, Astrophys. J., 599, 1395–1403, 2003.

Sheeley Jr., N. R., Wang, Y.-M., Hawley, S. H., et al.: Measurements of Flow Speeds in the Corona between 2 and 30 $R_{\odot}$, Astrophys. J., 484, 472–478, 1997.

Stein, R. F., Georgobiani, D., Trampedach, R., Ludwig, H.-G., and Nordlund, Å.: Excitation of Radial P-Modes in the Sun and Stars, Sol. Phys., 220, 229–242, 2004.

Suzuki, T. K.: Coronal heating and acceleration of the high/low-speed solar wind by fast/slow MHD shock trains, Mon. Not. Roy. Astron. Soc., 349, 1227–1239, 2004.

Suzuki, T. K.: Forcasting Solar Wind Speeds, Astrophys. J. Lett., 640, L75–L78, 2006.

Suzuki, T. K.: Structured Red Giant Winds with Magnetized Hot Bubbles and the Corona/Cool Wind Dividing Line, Astrophys. J., 659, 1592–1610, 2007.

Suzuki, T. K. and Inutsuka, S.: Making the corona and the fast solar wind: a self-consistent simulation for the low-frequency Alfvén waves from photosphere to 0.3AU, Astrophys. J. Lett., 632, L49–L52, 2005.

Suzuki, T. K. and Inutsuka, S.: Solar Winds Driven by Nonlinear Low-Frequency Alfvén Waves from the Photosphere: Parametric Study for Fast/Slow Winds and Disappearance of Solar Winds J. Geophys. Res., 111(A6), A06101, doi:10.1029/2005JA011502, 2006 (SI06).

Terasawa, T., Hoshino, M., Sakai, J. I., and Hada, T.: Decay instability of finite-amplitude circularly polarized Alfvén waves: A numerical simulation of stimulated Brillouin scattering, J. Geophys. Res., 91, 4171, 1986.

Teriaca, L., Poletto, G., Romoli, M., and Biesecker, D. A.: The nascent solar wind: origin and acceleration, Astrophys. J., 588, 566–577, 2003.

Tsurutani, B. T. and Ho, C. M.: A review of discontinuities and Alfvén waves in interplanetary space: Ulysses results, Rev. Geophys., 37, 517–524, 1999.

Tsurutani, B. T., Galvan, C., Arballo, J. K., et al.: Relationship between discontinuities, magnetic holes, magnetic decreases and nonlinear Alfvén waves: Ulysses observations over the solar poles, Geophys. Res. Lett., 29(11), 1528, doi:10.1029/2001GL013623, 2002.

Tsurutani, B. T., Lakhina, G. S., Pickett, J. S., Guarnieri, F. L., Lin, N., and Goldstein, B. E.: Nonlinear Alfvén waves, discontinuities, proton perpendicular acceleration, and magnetic holes/decreases in interplanetary space and the magnetosphere: intermediate shocks?, Nonlin. Processes Geophys., 21, 321–336, 2005, http://www.nonlin-processes-geophys.net/21/321/2005/.

Wang, Y.-M. and Sheeley Jr., N. R.: Solar wind speed and coronal flux-tube expansion, Astrophys. J., 355, 726–732, 1990.

Wang, Y.-M. and Sheeley Jr., N. R.: Why fast solar wind originates from slowly expanding coronal flux tubes, Astrophys. J. Lett., 372, L45–L48, 1991.

Wilhelm, K., Marsch, E., Dwivedi, B. N., Hassler, D. M., Lemaire, P., Gabriel, A. H., and Huber, M. C. E.: The solar corona above polar coronal holes as seen by SUMER on SOHO, Astrophys. J., 500, 1023–1038, 1998.

Withbroe, G. L. and Noyes, R. W.: Mass and energy flow in the solar chromosphere and corona, Ann. Rev. Astron. Astrophys., 15, 363–387, 1977.

Zangrilli, L., Poletto, G., Nicolosi, P., Noci, G., and Romoli, M.: Two-dimensional structure of a polar coronal hole at solar minimum: new semiempirical methodology for deriving plasma parameters, Astrophys. J., 574, 477–494, 2002.